Upper-body Impedance Control with Variable Stiffness for a Door Opening Task

Jinoh Lee[1], Arash Ajoudani[1], Enrico Mingo Hoffman[1], Alessio Rocchi[1], Alessandro Settimi[2], Mirko Ferrati[2], Antonio Bicchi[1,2], Nikolaos G. Tsagarakis[1], Darwin G. Caldwell[1]

***Abstract*— The advent of humanoids has brought new challenges in the real-world application. As a part of ongoing efforts to foster functionality of the robot accommodating a real environment, this paper introduces a recent progress on a door opening task with our compliant humanoid, CoMan. We presents a task-prioritized impedance control framework for an upper body system that includes a dual-arm, a waist, two soft hands, and 3D camera. Aimed to create desired responses to open the door, a novel stiffness modulation method is proposed, incorporating a realtime optimization. As a preliminary experiment, a full door-opening scenario (approaching to the door and reaching, grasping, rotating and pulling the door handle) is demonstrated under a semi-autonomous operation with a pilot. The experimental result shows the effectiveness and efficacy of the proposed impedance control approach. Despite of uncertainties from sensory data, the door opening task is successfully achieved and safe and robust interaction is established without creating excessive forces.**

I. INTRODUCTION

In past decades, natural/man-made disasters such as tragic collapse of World Trade Center in New York, Hanshin-Awajii earthquake in Kobe, and the earthquake, tsunami and subsequent problems at the Fukushima nuclear power plant have highlighted the need for robotic systems for effective disaster responses. This has led to practical robotics research which aims to execute tasks too hazardous for humans, for example, the DARPA Robotics Challenge (DRC) [1] and a European Commission-funded project, Whole-body Adaptive Locomotion and Manipulation, WALK-MAN [2].

One important step in this challenge is to interface the robot with the human world. To operate within infrastructures originally designed for humans, the robot should possess adaptive and robust manipulation skills. Of a large set of real world tasks, this paper focuses on developing a control framework for a multiple degrees-of-freedom (DOFs) humanoid with passive compliant joints to open a door. This will be achieved semi-autonomously by a "pilot."

Pioneering research on the door opening has been done by Nagatani et al.with a mobile manipulator, where the system can navigate paths to pass though a door way [3]. To enhance recognition of the environment for the manipulation, sensor-based control architectures have been incorporated using visual servoing [4] and multi-sensor fusion techniques [5]. However, the key difficulties in door opening mostly stem from the geometrical constraint created by the door, because inevitable kinematic errors and sensor uncertainties can potentially induce large internal forces between the door handle and an end-effector; these may damage the robot and/or the manipulated object. To reduce this problem, the authors in [6] proposed an online estimation algorithm for trajectory generation, and compliance/impedance control strategies have been proposed in [7], [8]. Building on this, the DRC encourages humanoids to be employed for the door opening task [9]–[11], since a humanoid is able to perform many high DOFs tasks in parallel, e.g., balancing, joint-limit avoidance, and self-collision avoidance.

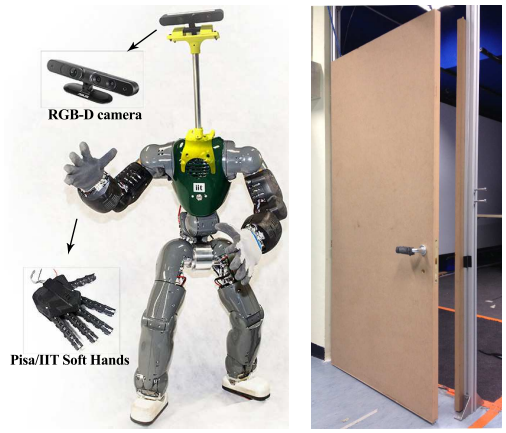

(a) (b)

Fig. 1: (a) The CoMan with an RGB-D carama and Pisa/IIT soft hands, and (b) a door with a spring-loaded handle.

In this paper, we report our recent accomplishment on the door opening task with the Compliant huManoid (CoMan) [12]–[14] depicted in Fig. 1, integrated with perception, manipulation, locomotion, and teleoperation with a graphic user interface (GUI). The main contribution is made to propose an impedance control strategy for upper-body manipulation to open the door by using an intuitive joint stiffness modulation method. This is undertaken within a teleoperation scenario based on simple motion primitives which is carefully balanced with an autonomous control.

The multiple DOFs in upper body often means that the robot must solve many subtasks in addition to the primary goal. In this paper, the primary task controls upper body

This work is supported by the the European Research Council, within the SAPHARI and the WALK-MAN projects. It is also partly supported by Basic Science Research Program through the National Research Foundation of Korea funded by the Ministry of Education (2013R1A6A3A03062246).

[1]The authors are with the Dept. of Advanced Robotics, Istituto Italiano di Tecnologia, Via Morego 30, 16163, Genova, Italy. [2]The authors are with Interdepartmental Research Centre "E. Piaggio", Faculty of Engineering, University of Pisa, Largo Lucio Lazzarino 1, 56122, Pisa, Italy

motion including dual arms and a waist, while the multiple subtasks are performed in the null space based on the task-priority [15]. To provide robust and stable interaction during the task, decentralized joint-impedance control is implemented into all joints. A novel online joint-stiffness planer, incorporating reatime optimization, is proposed to achieve the behaviors which enable CoMan to naturally adapt to geometric constraints imposed when opening the door.

II. SYSTEM DESCRIPTION

A. Hardware configuration

The CoMan, shown in Fig. 1 (a), is a fully torque-controlled robot with 29 DOFs, where 7 DOFs are in each arm, 3 DOFs in the waist, and 6 DOFs in each legs. This humanoid particularly has passive joint compliances which enhance physical interaction performance and self protection from high-bandwidth impact forces. The robot uses brushless DC motors and harmonic drives controlled with a Digital Signal Processor (DSP) located next to the actuator which runs the servo control firmware at 1 kHz in realtime and provides a torque-level controllers. Each joints measures position, velocity and torque, while there are also an inertial measurement unit (IMU) in the waist and four 6 axes force-torque sensors in the ankles and wrists. For a visual perception, an RGB-D (Red, Green, Blue plus Depth) camera, Asus Xtion Pro, is mounted above the torso to provide point cloud information.

To dexterously manipulate an object, CoMan is integrated with a Pisa/IIT SoftHand [16] shown in Fig. 1 (a), which is an anthropomorphic hand designed with 19 DOFs, where 4 DOFs on each of four fingers and 3 DOFs on the thumb are assigned. Based on the adaptive synergy approach [17], a single tendon runs through all joints to simultaneously flex and adduct the fingers upon actuation, that is, the hand is actuated by a single DC motor which moves the fingers on the path of the first synergy, allowing the physical hand to mold around the desired object. This provides simple yet robust grasping performance for manipulating the door handle as shown in Fig. 1 (b).

B. Software configuration

The semi-autonomous control architecture for the door opening task is depicted in Fig. 2. CoMan is controlled through a middleware framework YARP [18], while all the perception is handled by ROS [19]. Each DSP board at the joint implements decentralized joint position and impedance controls running, and the *RobotInterface* module uses the *Robolli* library to bring the low-level DSP functionalities to the YARP level.

The manipulation module (*open_door_module*) is written by using YARP functionalities, while the kinematic and dynamic model of the robot is specified using Unified Robot Description Format (URDF), parsed by the *IdynTree* library to obtain forward kinematics, Jacobians and dynamics computation. This module conforms to a simple communication protocol to control state transitions in an internal state machine. The visual perception module provides the position

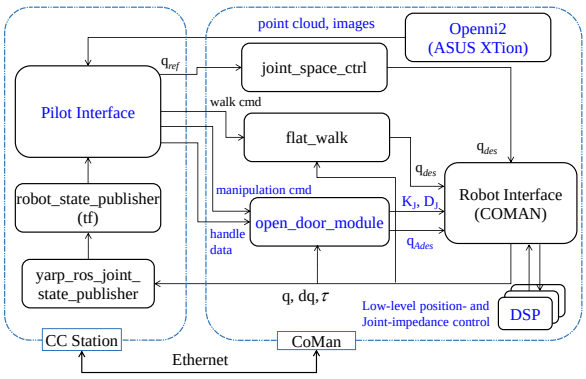

Fig. 2: Control system architecture for door opening task, where the CC station denotes Command-Control Station.

and orientation of the door handle with respect to the base reference frame which is sent to the YARP port to be used for trajectory generation. Finally, a *command* port accepts door-manipulation primitives to reach to the door handle, grasp, rotate, and pull it. The motion primitives commands are sent to the robot using the TCP protocol composed of strings and doubles.

III. TASK-PRIORITIZED FRAMEWORK FOR UPPER BODY

In this section, the control of the upper-body, including both arms and the waist joints, is introduced. This is achieved by creating prioritized-velocity commands for multiple tasks.

A. Upper-Body Kinematics

The schematic diagram of the upper-body manipulation system is illustrated in Fig. 3 with the joint-space vectors of the waist $\mathbf{q}_w \in \Re^3$, the right arm $\mathbf{q}_r \in \Re^7$ and the left arm $\mathbf{q}_l \in \Re^7$. The reference frames are defined as follows: the base frame Σ_o at the virtual floating base, the waist frame Σ_w, the torso frame Σ_t, the right-hand frame Σ_r, the left-hand frame Σ_l, and the camera frame Σ_c for the vision sensor.

The upper-body system is composed of two main kinematic chains for left and right arms with shared waist joints. For each kinematic chain, the first-order kinematic equations can be expressed as follows:

$$ {}^o\dot{\mathbf{x}}_r = {}^o\mathbf{J}_r \begin{bmatrix} \dot{\mathbf{q}}_w \\ \dot{\mathbf{q}}_r \end{bmatrix} = \begin{bmatrix} {}^o\mathbf{J}_{r|w} & {}^o\mathbf{J}_{r|wr} \end{bmatrix} \begin{bmatrix} \dot{\mathbf{q}}_w \\ \dot{\mathbf{q}}_r \end{bmatrix}, \quad (1) $$

$$ {}^o\dot{\mathbf{x}}_l = {}^o\mathbf{J}_l \begin{bmatrix} \dot{\mathbf{q}}_w \\ \dot{\mathbf{q}}_l \end{bmatrix} = \begin{bmatrix} {}^o\mathbf{J}_{l|w} & {}^o\mathbf{J}_{l|wl} \end{bmatrix} \begin{bmatrix} \dot{\mathbf{q}}_w \\ \dot{\mathbf{q}}_l \end{bmatrix}, \quad (2) $$

where the superscript denotes the reference frame, in this case, the base frame Σ_o; ${}^o\mathbf{x}_r \in \Re^6$ and ${}^o\mathbf{x}_l \in \Re^6$ denote position and orientation vectors of the right and left hands, respectively; ${}^o\mathbf{J}_r \in \Re^{6\times(3+7)}$ and ${}^o\mathbf{J}_l \in \Re^{6\times(3+7)}$ denote Jacobian matrices for the kinematic chains of the right and left arms from Σ_o, respectively; ${}^o\mathbf{J}_{r|w}, {}^o\mathbf{J}_{l|w} \in \Re^{6\times3}$ denotes the Jacobian matrix from Σ_o to the waist frame Σ_w for

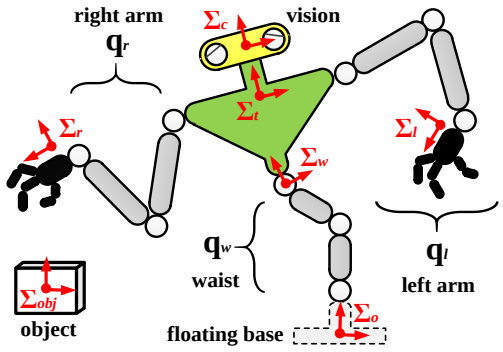

Fig. 3: Schematics of an upper-body manipulation system.

right and left branches, respectively; ${}^o\mathbf{J}_{r|wr} \in \Re^{6\times7}$ and ${}^o\mathbf{J}_{l|wl} \in \Re^{6\times7}$ are Jacobian matrices from Σ_w to Σ_r and Σ_l, respectively; and $\mathbf{q}_w \in \Re^3$, $\mathbf{q}_r \in \Re^7$ and $\mathbf{q}_l \in \Re^7$ are joint space vectors of the waist, right arm and left arm, respectively. Hereafter, for brevity the superscript o describing the base frame is omitted.

A task vector in the operational space of the upper-body can be defined by the position/orientation of two end-effectors as $\mathbf{x}_A = \begin{bmatrix} \mathbf{x}_r^T & \mathbf{x}_l^T \end{bmatrix}^T \in \mathbb{R}^{12}$. Considering that the waist joints are shared with two kinematic chains, one can derive the operational velocity vector through the action of the upper-body Jacobian, $\mathbf{J}_A \in \Re^{12\times17}$, on the joint space vector $\dot{\mathbf{q}}_A \in \Re^{17} = \begin{bmatrix} \dot{\mathbf{q}}_w^T & \dot{\mathbf{q}}_r^T & \dot{\mathbf{q}}_l^T \end{bmatrix}^T$ as follows:

$$\dot{\mathbf{x}}_A = \mathbf{J}_A \dot{\mathbf{q}}_A, \tag{3}$$

where the expression of $\mathbf{J}_A$ can be derived from the individual Jacobians, that is,

$$\dot{\mathbf{x}}_A = \begin{bmatrix} \dot{\mathbf{x}}_r \\ \dot{\mathbf{x}}_l \end{bmatrix} = \underbrace{\begin{bmatrix} \mathbf{J}_{r|w} & \mathbf{J}_{r|wr} & \mathbf{0} \\ \mathbf{J}_{l|w} & \mathbf{0} & \mathbf{J}_{l|wl} \end{bmatrix}}_{\mathbf{J}_A} \begin{bmatrix} \dot{\mathbf{q}}_w \\ \dot{\mathbf{q}}_r \\ \dot{\mathbf{q}}_l \end{bmatrix}. \tag{4}$$

B. Task-Prioritization

In the framework of resolved rate control, a general inverse solution to the differential kinematic mapping (3) is obtained as

$$\dot{\mathbf{q}}_A = \mathbf{J}_A^\dagger \dot{\mathbf{x}}_A + \dot{\mathbf{q}}_s, \tag{5}$$

where $\mathbf{J}_A^\dagger$ denotes the Moore-Penrose pseudo-inverse [20] of $\mathbf{J}_A$, $\dot{\mathbf{q}}_s$ denotes a joint velocity for subtasks projected onto the null-space.

Note that in this paper, since we particularly take care of the door manipulation task in a *semi-autonomous* manner, the *pilot* is supposed to select one hand to manipulate a door handle, i.e., the hand closer to the handle. Thus we suggest that a simple and intuitive way to manage the selection of arms and to avoid kinematic singularity is the use of weighted-damped least-square inverse resolution, that is,

$$\begin{cases} \mathbf{J}_A^{W\#} = \mathbf{W}^{-1}\mathbf{J}_A^T(\mathbf{J}_A\mathbf{W}^{-1}\mathbf{J}_A^T + \lambda\mathbf{I}_{17})^{-1} \\ \mathbf{W} \triangleq diag\begin{bmatrix} \mathbf{W}_w & \mathbf{W}_w & \mathbf{S}_r & \mathbf{S}_l \end{bmatrix}, \end{cases} \tag{6}$$

where $\mathbf{W}_w \in \Re^{3\times3}$ denotes a diagonal matrix to weigh the contribution of waist motion to the upper-body motion, $\mathbf{S}_r, \mathbf{S}_l \in \Re^{7\times7}$ denote selection matrices chosen by the pilot, i.e., $\mathbf{I}_7$ or $\mathbf{0}_7$, where the subscript denotes the dimension of identity and zero matrices, and $\lambda>0$ denotes the damped least square gain.

Assuming that there are k subtasks, where the i-th subtask has lower priority than the $(i-1)$-st subtask such that i=1, . . . , k, the i-th subtask can be represented by the coordinate vector, $\mathbf{x}_i \in \Re^{m_i}$ where m_i denotes the DOFs of the i-th subtask. Its associated i-th subtask Jacobian is presented by $\mathbf{J}_i \in \Re^{m_i\times17} = \partial\mathbf{x}_i/\partial\mathbf{q}_A$. Then, based on the use of the task-priority approach [15] for the multiple subtasks, the resolved velocity of the subtasks is defined as

$$\dot{\mathbf{q}}_s = \sum_{i=1}^{k} \dot{\mathbf{q}}_i + \mathbf{N}_k\boldsymbol{\xi}, \tag{7}$$

where $\dot{\mathbf{q}}_i \in \Re^{17}$ denotes the resolved joint velocity of the i-th subtask, and is given by

$$\dot{\mathbf{q}}_i = (\mathbf{J}_i\mathbf{N}_i)^\#(\dot{\mathbf{x}}_i - \mathbf{J}_i\sum_{j=1}^{i-1}\dot{\mathbf{q}}_{N(i)}), \quad \dot{\mathbf{q}}_{N(1)} = \mathbf{0}, \tag{8}$$

where $\mathbf{N}_i$ denotes the null-space projection matrix of the i-th subtask [21], the superscript $\#$ denotes a damped least-squares inverse [22], which is defined as $\mathbf{A}^\# = \mathbf{A}^T(\mathbf{A}\mathbf{A}^T + \lambda\mathbf{I})^{-1}$. In the second term of the right-hand side of (7), $\boldsymbol{\xi}$ denotes an arbitrary velocity term for self motion. In this paper, we use this term to achieve joint-limits avoidance. To efficiently avoid the joint limit in real-time, a classic local optimization based on the gradient projection method (GPM) is applied as follows:

$$\boldsymbol{\xi} = \alpha\nabla V(\mathbf{q}_A), \tag{9}$$

$$V(\mathbf{q}_A) = \frac{1}{4}\sum_{i=1}^{n}\frac{(q_{i,\max} - q_{i,\min})^2}{(q_{i,\max} - q_i)(q_i - q_{i,\min})}, \tag{10}$$

where $\alpha > 0$ is a suitable scalar stepsize for GPM, and q_{max} and q_{min} denote the upper and lower limits of i-th joint, respectively.

Indeed, the joint motion reference $\mathbf{q}_{Ades}\in\Re^{17}$ for the upper body induced from the operational motion reference $\mathbf{x}_{Ades}\in\Re^{12}$ is created by the inverse solution, (5). To mitigate the numerical drift problem of inverse kinematics solutions, a closed-loop inverse kinematic (CLIK) algorithm is implemented [23]. Combining (5)-(9), the final kinematic control equation based on CLIK yields

$$\begin{aligned} \dot{\mathbf{q}}_{Ades} = {} & \mathbf{J}_A^{W\#}(\dot{\mathbf{x}}_{Ades} + \mathbf{K}_c\mathbf{e}_A) \\ & + \sum_{i=1}^{k}(\mathbf{J}_i\mathbf{N}_i)^\#(\dot{\mathbf{x}}_i - \mathbf{J}_i\sum_{j=1}^{i-1}\dot{\mathbf{q}}_{N(i)}) + \mathbf{N}_k\boldsymbol{\xi}, \end{aligned} \tag{11}$$

where $\mathbf{e}_A \triangleq (\mathbf{x}_{Ades} - \mathbf{x}_A)$ is the task-space error; note that in (11), CLIK can be also applied to the subtasks $\mathbf{x}_i$ [24].

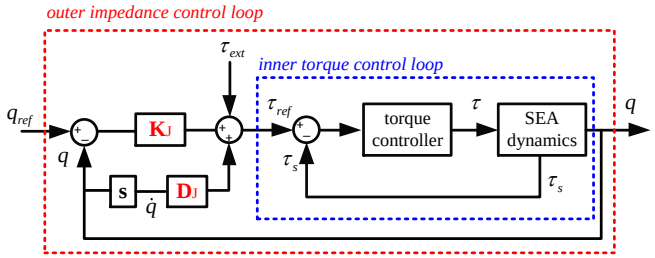

Fig. 4: Block diagram of the low-level controller with inner toque control loop and outer impedance control loop.

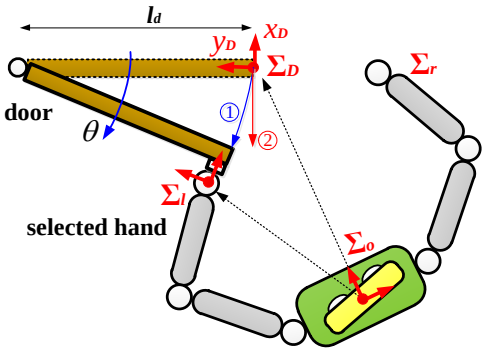

Fig. 5: Schematic diagram of the door manipulation: l_d and θ denote the width and opening angle of the door, the blue arrow with ① denotes an accurate end-point path of the door, and the red arrow with ② denotes an end-point path perpendicular to the door frame.

IV. IMPEDANCE CONTROL FOR OPENING DOOR

Difficulties during the door opening mostly originate from inability to generate an appropriate end-effector path due to uncertainty and inaccuracy in the sensory data. In this section, instead of creating a precise trajectory, we strive to find a more intuitive way to control the upper body system, based on an impedance control strategy offering a compliant behavior with a joint-stiffness modulation allowing the robot to naturally adapt to interaction forces between itself and the door.

A. Decentralized Joint-Impedance Control

As briefly introduced in Section II-A, CoMan has a passive (and active) compliance at the joints due to series elastic actuators (SEA), where the dynamic model can be expressed as follows:

$$\begin{cases} \mathbf{M}_L\ddot{\mathbf{q}}_L + \mathbf{c}_L(\mathbf{q}_L, \dot{\mathbf{q}}_L) + \mathbf{f}_L + \mathbf{g}_L + \mathbf{K}(\mathbf{q}_L - \mathbf{q}) = \boldsymbol{\tau}_L, \\ \mathbf{M}\ddot{\mathbf{q}} + \mathbf{c}(\mathbf{q}, \dot{\mathbf{q}}) + \mathbf{f} + \mathbf{K}(\mathbf{q} - \mathbf{q}_L) = \boldsymbol{\tau}, \end{cases} \tag{12}$$

where the subscript $\bullet_L$ denotes the link-side variable, $\mathbf{M}$ denotes the inertia matrix, $\mathbf{c}$ denotes a vector of Coriolis and centrifugal forces, $\mathbf{f}$ denotes a vector of a frictional force, $\mathbf{g}$ represents a gravitational force vector and $\mathbf{K}$ denotes a diagonal matrix of physical joint stiffness in SEA, finally $\boldsymbol{\tau}_L$ denotes a torque exerted on the link. The joint torque, $\boldsymbol{\tau}_s = \mathbf{K}(\mathbf{q} - \mathbf{q}_L)$, is measured by customized strain gauges in the SEA.

The joints use a decentralized impedance controller with its control law represented by

$$\boldsymbol{\tau}_{ref} = \boldsymbol{\tau}_c + \mathbf{K}_J(\mathbf{q}_{ref} - \mathbf{q}) - \mathbf{D}_J\dot{\mathbf{q}}, \tag{13}$$

where $\boldsymbol{\tau}_{ref}$ denotes the reference torque which creates joint stiffness $\mathbf{K}_J$, and joint damping $\mathbf{D}_J$, and $\boldsymbol{\tau}_c$ denotes an external torque to be compensated, e.g., the gravitational torque. The corresponding block diagram is illustrated in Fig. 4. The outer impedance loop provides a reference torque command to the inner torque control loop, where proportional-integral (PI) torque control is usually chosen for simplicity. The PI gains can be tuned to achieve the highest possible bandwidth and to ensure the passivity and stability of the overall system; it is experimentally verified that this satisfies $K_J \in (0\ \ 2000]$ and $D_J \in (0\ \ 30]$ (See more details in [25].) This joint-impedance controller is implemented on the low-level DSPs located in each joints as shown in Fig. 2, while the high-level controller on the on-board PC emulates the joint stiffness, $\mathbf{K}_J$ where the methodology is proposed in the following subsection.

B. Joint Stiffness Emulation For Opening a Door

To plan an appropriate compliant behavior for the door opening task, we first define a desired Cartesian stiffness with respect to the door frame, ${}^D\mathbf{K}_{des} \in \Re^{6\times6}$. Inspired by human actions in door opening, the robot compliance is used to drive the robot behavior. However, people do not consciously control their each joint stiffnesses, but try to adjust their body actions depending on the task. For example, the task frame in this case is the door frame attached at the handle as shown in Fig. 5; then, it is natural that stiffer motion is required perpendicular to the door handle, x_D-axis, to apply more force and in the rotational direction along x_D-axis to maintain the rotation angle of the handle, while compliant motion is required in the other directions to smoothly reduce the interaction forces between the handle and the robot. From this observation, we propose an joint-stiffness $\mathbf{K}_J$ in (13) is emulated from ${}^D\mathbf{K}_{des}$, i.e., with respect to the door frame.

Once the pilot selects the manipulating arm for the door opening, the selected joint vector $\mathbf{q} \in \Re^{10}$ can be determined as $\mathbf{q} = [\ \mathbf{q}_w^T \ \ \mathbf{q}_r^T\ ]^T\ [\ \mathbf{q}_w^T \ \ \mathbf{q}_l^T\ ]^T$ for right or left kinematic chains, respectively; the selected Jacobian with respect to the base frame $\mathbf{J} \in \Re^{6\times10}$ can be defined as $\mathbf{J} = \mathbf{J}_{r|wr}$ or $\mathbf{J} = \mathbf{J}_{l|wl}$, for right or left kinematic chains, respectively.

The relationship between the force acting on the door handle referenced from the door frame, Σ_D, and the joint torques required to produce this force can be obtained by applying the principle of virtual work. Equating the work, δW_τ, done by the joint displacements, $\delta\mathbf{q}$, can be expressed as

$$\delta W_\tau = \boldsymbol{\tau}_q^T \delta\mathbf{q}, \tag{14}$$

where $\boldsymbol{\tau}_q$ denotes the corresponded joint torques; and the work, δW_f, done by the forces acting on the door with

respect to the door frame, ${}^{D}\mathbf{f}$, can be given as

$$\delta W_f = {}^{D}\mathbf{f}^T \delta {}^{D}\mathbf{x}, \tag{15}$$

where $\delta {}^{D}\mathbf{x}$ denotes the displacement of the door handle with respect to the door frame. Assuming the end-effector firmly grasps the door handle, substituting (15) into (14) yields

$$\boldsymbol{\tau}_q = (\delta {}^{D}\mathbf{x}/\delta \mathbf{q})^T {}^{D}\mathbf{f} = {}^{D}\mathbf{J}^T {}^{D}\mathbf{f}, \tag{16}$$

where ${}^{D}\mathbf{J}$ is the Jacobian of the selected arm expressed in the door frame which is calculated as follows:

$${}^{D}\mathbf{J} = \begin{bmatrix} \mathbf{R}_D^T & \mathbf{0}_3 \\ \mathbf{0}_3 & \mathbf{R}_D^T \end{bmatrix} \mathbf{J}. \tag{17}$$

As above, the primary interest is the desired Cartesian stiffness with respect to the door frame, ${}^{D}\mathbf{K}_{des}$ to obtain suitable joint stiffnesses. This can be expressed in the following relationship between force and displacement:

$${}^{D}\mathbf{f} = {}^{D}\mathbf{K}_{des} \delta {}^{D}\mathbf{x}. \tag{18}$$

Substituting (18) into (16) gives

$$\boldsymbol{\tau}_q = {}^{D}\mathbf{J}^T {}^{D}\mathbf{K}_{des} \delta {}^{D}\mathbf{x} = ({}^{D}\mathbf{J}^T {}^{D}\mathbf{K}_{des} {}^{D}\mathbf{J}) \delta \mathbf{q}. \tag{19}$$

Therefore, we can derive the desired joint-space stiffness for the door manipulation from the desired Cartesian stiffness ${}^{D}\mathbf{K}_{des}$ as

$$\mathbf{K}_{Jdes} = {}^{D}\mathbf{J}^T {}^{D}\mathbf{K}_{des} {}^{D}\mathbf{J} \in \Re^{17\times 17}, \tag{20}$$

where $\mathbf{R}_D^T$ denotes the rotation matrix of the door frame with respect to the base frame which can be obtained from the head mounted RGB-D camera and the perception module.

It is important to notice that although the desired Cartesian stiffness matrix ${}^{D}\mathbf{K}_{des}$ can be arbitrarily set, it is typically a diagonal matrix due to its clearer meaning in three positional and three rotational directions. whereas, in our application the joint stiffness is implemented by the joint-impedance controller at each joint; therefore the joint stiffness matrix $\mathbf{K}_J$ in (13) is represented as a diagonal matrix. This diagonality of $\mathbf{K}_J$ creates an inherent limitation in the desired joint stiffness matrix $\mathbf{K}_{Jdes}$ because it is non-diagonal, as shown in (20).

To mitigate this limitation, we formulate an optimization problem in the similar manner to [26] as follows:

$$\min_{\mathbf{k}_J} ||\mathbf{K}_J(\mathbf{k}_J) - {}^{D}\mathbf{J}^T {}^{D}\mathbf{K}_{des} {}^{D}\mathbf{J}||_F^2, \tag{21}$$

where $\mathbf{K}_J(\mathbf{k}_J) \in \Re^{10\times 10}$ denotes the diagonal matrix with joint-stiffness values of $\mathbf{k}_J \in \Re^{10}$, and the matrix norm is defined as

$$||\mathbf{X}||_F = (\sum_{i=1}^{m}\sum_{j=1}^{n} |x_{ij}|^2)^{\frac{1}{2}} \tag{22}$$

which is the Frobenius norm of $\mathbf{X} \in \Re^{m\times n}$. In this paper, to obtain a reliable solution in realtime, a local optimization was done using Levenberg–Marquardt algorithm implemented from "ALGLIB" optimization library [27]. The experimental result of the stiffness optimization is shown in Section V-A.

C. Discussion on the Trajectory Generation

In the beginning of the operation, the RGB-D camera collects the position and orientation of the door handle with respect to the camera frame, Σ_c. Through the pilot interface as shown in Fig. 2, the trajectory generator receives the door-handle data which is coordinate-transformed to the based frame, Σ_o.

To create an accurate path for opening the door such as the blue arrow with ① in Fig. 5, one needs a very good approximation of the door length l_d. However, since the robot has to stand close to the door for grasping its handle, it is quite difficult to obtain l_d from an RGB-D type camera. In addition, to precisely estimate l_d, sophisticated estimation methods may be needed as well. On the other hands, when observing human door opening behaviour, one may not need such an information. It can be intuitively assumed that humans apply a force to open the door after grasping the handle and naturally adapt the configuration of the arm (or body) with a certain level of compliance against the geometric constraints from the door.

Therefore, in this paper, we generate a fifth-order polynomial trajectory based on the door data from the pilot interface (the initial position/orientation of the door handle), for instance, the red arrow ② in Fig. 5. This is a roughly approximated trajectory for the door handle. Nevertheless, once the desired stiffness is emulated as shown in the previous subsection, the end-effector can be smoothly and compliantly adapted to the geometric constraint of the door preventing high interaction forces at the end-effector. Because this trajectory generation only requires door data once, at the beginning of the operation, it is easily implemented in realtime control. The deficiency of the trajectory modeling is compensated by the implemented joint stiffness.

V. EXPERIMENTS

A. Door Opening Demonstration

Figure 6 shows the whole door opening experiment which is commanded by the operator using the pilot interface shown in Fig. 7. The pilot interface consists of three major components: a 2D image window showing realtime camera views; a 3D robot configuration window providing the point-cloud data and actual robot posture; and a command window offering motion primitives buttons for walking and for manipulating the door.

In the demonstration, the pilot first recognizes the position of the door through the 2D image and commands the robot to approach to the door through the "walking" module, *flat_walk* depicted in Fig. 2. After the robot reaches the door, the door handle data is identified from the 3D point cloud of the scene and the hand is selected to grasp the handle. Then, the motion primitives *Grasping*, *Turning*, *Opening*, *Supporting*, and *Ungrasping* are sequentially directed by the pilot.

Each motion primitive is autonomously controlled within the task-priority based framework shown in (11). The weighted damped-least-square solution of the inverse kinematics, shown in (6), provides robustness to singularities. If

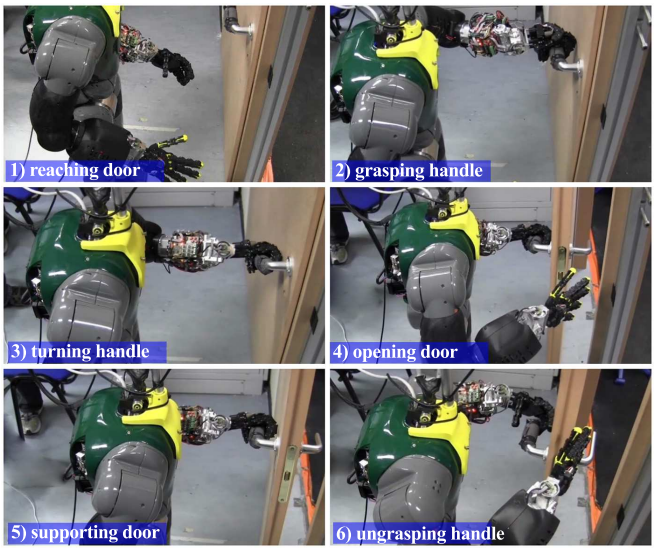

Fig. 6: The snapshots of the door opening experiment.

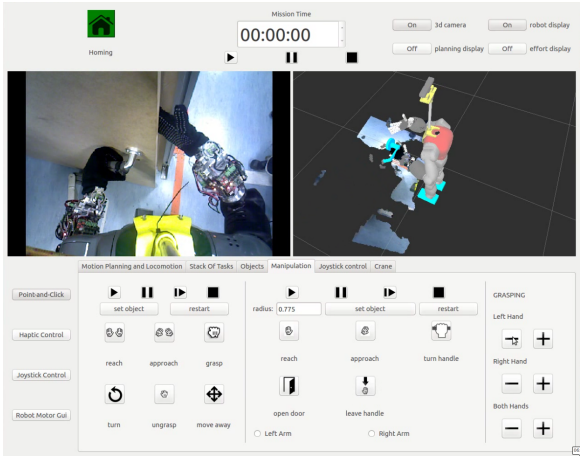

Fig. 7: The pilot interface: a 3D handle model is overlaid on the 3D scene, and commands are sent from a GUI.

the pilot selects the left arm, the selection matrices are set as $\mathbf{S}_r = \mathbf{0}_7$ and $\mathbf{S}_l = \mathbf{I}_7$. Note that in this experimental setup, the lower-body locomotion and upper-body manipulation modules are independent. To maintain the balance of the whole body, while the locomotion module stabilizes lower-body balance against various perturbations, the weighting matrix of the waist is set as $\mathbf{W}_w = 0.1\mathbf{I}_3$ to attenuate severe change of the center of mass of the upper-body. In addition, the joint-limit avoidance was achieved in the null space of the upper-body Jacobian.

Throughout the demonstration, it is verified that the tele-operation scenario based on semi-autonomous control indeed can provide quick task fulfillment. It takes 75 seconds for the execution of the task shown in Fig 6.

B. Experimental Results

To verify the effectiveness of the proposed impedance control strategy with the varying stiffness, we have investigated the control result during the execution of motion primitive

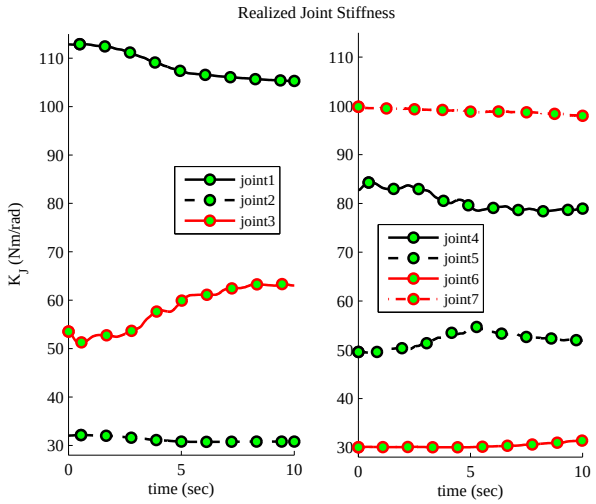

Fig. 8: The plot of the joint stiffness $\mathbf{k}_J$ emulated from the desired Cartesian stiffness ${}^D\mathbf{K}_{des}$.

Opening. Since none of a spring and a damper is loaded in the current door setup, weights of 4 kg in total are put on the ground which meet the end of the door tip; this may create a resistance force to the door similar to the action of the spring-damper loaded door.

The desired Cartesian stiffness with respect to the door frame is set as

$$ {}^D\mathbf{K}_{des} = \mathrm{diag}\{500, 100, 100, 150, 30, 30\}, \qquad (23) $$

where the first element implements the stiff behavior along x_D-axis (the direction perpendicular to the door handle) which overcomes the resistance forces to open the door, the fourth element implements the stiff rotational behavior along x_D-axis to sustain the angle of the spring-loaded handle, and the other elements implement compliant behaviors for the hand to accommodate the geometric constraint caused by the discrepancy of the trajectory and other uncertainties. The joint damping is set as a constant value of 6 Nms/rad for all joints.

Figure 8 shows the stiffness elements of seven joints in the left arm realized into the joint impedance controller which are firstly calculated from (20) and then locally optimized by (21) in realtime execution. To confirm the optimized joint stiffness can realize the desired behavior for the door opening, the force response measured at the end-effector is displayed in Fig. 9. In particular, the results are compared with those of a joint-position controller which produces stiff motion in all direction, so as to clearly show the efficacy of the proposed control strategy.

In Fig. 9, one can observe that the force response of impedance controller along x_D-axis increases in order to create enough force to open the door, and it is similar to that of position control. Whereas, in the force response along y_D- and z_D-axes, the impedance controller induces the smaller interaction forces, i.e., 32.24 % in y_D-axis and 31.16 % in z_D-axis compared to that of position controller. These results

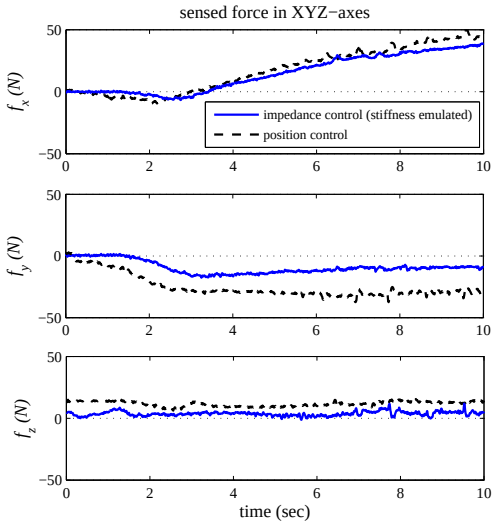

Fig. 9: The plot of the force responses between the hand and the door handle.

clearly demonstrate that the realized stiffnesses of each joint successfully generate the desired stiff motion in x_D-axis and the compliant motions in y_D- and z_D-axes, yet no excessive interaction forces at the end-effector.

VI. CONCLUSION AND FUTURE WORKS

This paper has shown the recent progress of humanoid robot CoMan performing a door-opening task with a preliminary demonstration. A task-prioritized control framework for multiple DOFs upper body is derived based on the analysis of dual arm and the waist kinematics. On top of this, a joint stiffness modulation scheme is proposed for the humanoid to robustly and safely interact with the door, incorporating a joint-level impedance controller and a local optimization for a realtime operation. It is worthwhile to address that although the decentralized joint impedance control strategy and CoMan's intrinsic compliance with SEAs involve safety of the robot from a damage, we have noticed that self-collision avoidance is still heavily required. Accordingly, an efficient realtime algorithm based on the proposed framework with a high priority will be implemented in our further work.

REFERENCES

[1] E. Ackerman, "DARPA robotics challenge trials: What you should (and shouldn't) expect to see," *IEEE Spectrum*, vol. 19, 2013.

[2] WALK-MAN Project. (2014) Whole-body adaptive locomotion and manipulation. [Online]. Available: http://www.walk-man.eu/

[3] K. Nagatani and S. Yuta, "Designing a behavior of a mobile robot equipped with a manipulator to open and pass through a door," *Robotics and autonomous systems*, vol. 17, no. 1, pp. 53–64, 1996.

[4] U. D. Hanebeck, C. Fischer, and G. Schmidt, "Roman: A mobile robotic assistant for indoor service applications," in *Proc. 1997 IEEE/RSJ Int. Conf. Intelligent Robots and Systems*, vol. 2, 1997, pp. 518–525.

[5] M. Prats, P. J. Sanz, and A. P. Del Pobil, "Reliable non-prehensile door opening through the combination of vision, tactile and force feedback," *Autonomous Robots*, vol. 29, no. 2, pp. 201–218, 2010.

[6] L. Peterson, D. Austin, and D. Kragic, "High-level control of a mobile manipulator for door opening," in *Proc. 2000 IEEE/RSJ Int. Conf. Intelligent Robots and Systems*, vol. 3, 2000, pp. 2333–2338.

[7] G. Niemeyer and J.-J. Slotine, "A simple strategy for opening an unknown door," in *Proc. 1997 IEEE Int. Conf. Robotics and Automation*, vol. 2, 1997, pp. 1448–1453.

[8] C. C. Kessens, J. B. Rice, D. C. Smith, S. J. Biggs, and R. Garcia, "Utilizing compliance to manipulate doors with unmodeled constraints," in *Proc. 2010 IEEE/RSJ Int. Conf. Intelligent Robots and Systems*, 2010, pp. 483–489.

[9] H. Arisumi, J.-R. Chardonnet, and K. Yokoi, "Whole-body motion of a humanoid robot for passing through a door-opening a door by impulsive force," in *Proc. 2009 IEEE/RSJ Int. Conf. Intelligent Robots and Systems*, 2009, pp. 428–434.

[10] Y. Karayiannidis, C. Smith, F. E. Vina, P. Ogren, and D. Kragic, ""open sesame!" adaptive force/velocity control for opening unknown doors," in *Proc. 2012 IEEE/RSJ Int. Conf. Intelligent Robots and Systems*, 2012, pp. 4040–4047.

[11] M. Zucker, Y. Jun, B. Killen, T.-G. Kim, and P. Oh, "Continuous trajectory optimization for autonomous humanoid door opening," in *Proc. 2013 IEEE Int. Conf. Technologies for Practical Robot Applications*, 2013, pp. 1–5.

[12] N. G. Tsagarakis, S. Morfey, G. Medrano Cerda, L. Zhibin, and D. G. Caldwell, "Compliant humanoid coman: Optimal joint stiffness tuning for modal frequency control," in *Proc. 2013 IEEE Int. Conf. Robotics and Automation*, 2013, pp. 673–678.

[13] J. Lee, H. Dallali, N. Tsagarakis, and D. Caldwell, "Robust and model-free link position tracking control for humanoid coman with multiple compliant joints," in *Proc. 2013 IEEE Int. Conf. Humanoid Robots, Atlanta, Georgia, USA*, 2013, pp. 1–7.

[14] E. Spyrakos-Papastavridis, G. A. Medrano-Cerda, N. G. Tsagarakis, J. S. Dai, and D. G. Caldwell, "A push recovery strategy for a passively compliant humanoid robot using decentralized lqr controllers," in *Proc. 2013 IEEE Int. Conf. Mechatronics*, 2013, pp. 464–470.

[15] Y. Nakamura, H. Hanafusa, and T. Yoshikawa, "Task-priority based redundancy control of robot manipulators," *The International Journal of Robotics Research*, vol. 6, no. 2, pp. 3–15, 1987.

[16] M. G. Catalano, G. Grioli, E. Farnioli, A. Serio, C. Piazza, and A. Bicchi, "Adaptive synergies for the design and control of the Pisa/IIT softhand," *The International Journal of Robotics Research*, vol. 33, no. 5, pp. 768–782, 2014.

[17] A. Bicchi, M. Gabiccini, and M. Santello, "Modelling natural and artificial hands with synergies," *Philosophical Transactions of the Royal Society B: Biological Sciences*, vol. 366, no. 1581, pp. 3153–3161, 2011.

[18] G. Metta, P. Fitzpatrick, and L. Natale, "YARP: Yet another robot platform," *International Journal of Advanced Robotics Systems, special issue on Software Development and Integration in Robotics*, vol. 3, no. 1, 2006.

[19] M. Quigley, K. Conley, B. P. Gerkey, J. Faust, T. Foote, J. Leibs, R. Wheeler, and A. Y. Ng, "ROS: an open-source robot operating system," in *ICRA Workshop on Open Source Software*, 2009.

[20] A. Ben-Israel and T. N. Greville, *Generalized inverses*. Springer, 2003, vol. 13.

[21] J. Lee, P. H. Chang, and R. S. Jamisola, "Relative task prioritization for dual-arm with multiple, conflicting tasks: Derivation and experiments," in *Proc. 2013 IEEE Int. Conf. Robotics and Automation*, 2013, pp. 1928–1933.

[22] S. Chiaverini, B. Siciliano, and O. Egeland, "Review of the damped least-squares inverse kinematics with experiments on an industrial robot manipulator," *IEEE Trans. Contr. Syst. Technol.*, vol. 2, no. 2, 1994.

[23] S. Chiaverini, "Singularity-robust task-priority redundancy resolution for real-time kinematic control of robot manipulators," *IEEE J. Robot. Automat.*, vol. 13, no. 3, pp. 398–410, 1997.

[24] G. Antonelli, "Stability analysis for prioritized closed-loop inverse kinematic algorithms for redundant robotic systems," *IEEE Trans. Robot.*, vol. 25, no. 5, pp. 985–994, 2009.

[25] M. Mosadeghzad, G. Medrano-Cerda, J. Saglia, N. Tsagarakis, and D. Caldwell, "Comparison of various active impedance control approaches, modeling, implementation, passivity, stability and trade-offs," in *Proc. 2012 IEEE/ASME Int. Conf. Advanced Intelligent Mechatronics*, July 2012, pp. 342–348.

[26] F. Petit and A. Albu-Schaffer, "Cartesian impedance control for a variable stiffness robot arm," in *Proc. 2011 IEEE/RSJ Int. Conf. Intelligent Robots and Systems*, 2011, pp. 4180–4186.

[27] ALGLIB Project. (2014) ALGLIB®—numerical analysis library. [Online]. Available: http://www.alglib.net